Proc. Natl. Acad. Sci. USA
Vol. 93, pp. 2926–2929, April 1996
Biophysics

Imaging of single molecule diffusion

(fluorescence microscopy/single dye detection/time-resolved imaging/quantal fluorescence/lipid bilayers)

TH. SCHMIDT, G. J. SCHÜTZ, W. BAUMGARTNER, H. J. GRUBER, AND H. SCHINDLER

Institute for Biophysics, University of Linz, 4040 Linz, Austria

Communicated by George Feher, University of California, San Diego, La Jolla, CA, December 18, 1995 (received for review August 14, 1995)

ABSTRACT **In recent years observations at the level of individual atoms and molecules became possible by microscopy and spectroscopy. Imaging of single fluorescence molecules has been achieved but has so far been restricted to molecules in the immobile state. Here we provide methodology for visualization of the motion of individual fluorescent molecules. It is applied to imaging of the diffusional path of single molecules in a phospholipid membrane by using phospholipids carrying one rhodamine dye molecule. For this methodology, fluorescence microscopy was carried to a sensitivity so that single fluorescent molecules illuminated for only 5 ms were resolvable at a signal/noise ratio of 28. Repeated illuminations permitted direct observation of the diffusional motion of individual molecules with a positional accuracy of 30 nm. Such capability has fascinating potentials in bioscience—for example, to correlate biological functions of cell membranes with movements, spatial organization, and stoichiometries of individual components.**

The ultimate goal of high-sensitivity detection schemes is observation on the single molecule level. This came into reach by the invention of scanning probe microscopy (1, 2), which has since brought a wealth of new insights (3). Optical methods allowed for detection of single atoms (4). The effective light conversion in fluorescent molecules made it possible to detect single fluorophores in liquids by confocal fluorescence microscopy (5–8) and to perform high-resolution spectroscopy of single dye molecules at low temperature (9–12). The first true imaging of single dye molecules by optical means was achieved by scanning near-field optical microscopy (13). This method is unique in reaching a spatial resolution of ≈14 nm, much below the optical diffraction limit but restricted in its application to immobile objects. Very recently, single fluorescence labeled myosin molecules on immobilized actin filaments were imaged by conventional microscopy and illumination times of seconds (14).

It would be of interest for many applications, especially in bioscience, to extend microscopy to visualization of single fluorophores in motion. To our knowledge, such imaging has not been reported to date. Here we show that the motion of single dye molecules can be visualized by conventional fluorescence microscopy by extending the time resolution into the millisecond range. For this, we used epifluorescence microscopy with argon-ion laser excitation and imaging onto a highly-sensitive liquid-nitrogen-cooled CCD-camera. Optical parts were carefully selected to achieve an efficiency for the detection of emitted fluorescence as high as 3%, while scattered light was blocked effectively. For demonstration of the potentials of observing individual mobile molecules we have chosen a fluorescence-labelled lipid in a fluid lipid membrane as a most appropriate system. It uniquely permitted to use results obtained at high surface densities of labelled lipid for quantitative control in identifying isolated signals with single fluorescence-labelled lipids observed at low surface densities.

MATERIALS AND METHODS

Phospholipid Membranes. The lipids palmitoyloleoylphosphocholine (POPC, Avanti Polar Lipids) and *N*-(6-tetramethylrhodaminethiocarbamoyl)-1,2-dihexadecanoyl-*sn*-glycero-3-phosphoethanolamine, triethylammonium salt (TRITC DHPE; T-1391, Molecular Probes) were used without further purification. Lipid monolayers were generated at the air/buffer interface (buffer; 100 mM NaCl/10 mM NaH_2PO_4, pH 7.5) in a monolayer trough (Mayer Feintechnik, Göttingen, Germany) and held at 30 mN/m surface pressure. Lipid bilayers were deposited onto 0.17-mm-thick glass substrates by a Langmuir-Blodgett technique (15). Before use the substrates were cleaned with chromic acid and extensively washed in water. For bilayer formation a POPC monolayer on the glass substrate was horizontally apposed to a POPC monolayer at the air/buffer interface containing TRITC DHPE at a defined molar ratio. The molar ratio [TRITC DHPE]/[POPC] was varied between 6.5×10^{-9} and 6.5×10^{-4} mol/mol, which yielded a range of surface density of TRITC DHPE from 10^{-2} to 10^3 dyes/μm^2, assuming 0.63 nm^2 surface area per lipid (16). The lipid bilayer on the substrate was pushed through the air/buffer interface and clamped under water to an open quartz cell of 10 μm optical path length (136QS, Hellma). This cell was mounted on the microscope stage.

Fluorescence Microscopy. We used a Zeiss microscope (Axiovert 135-TV) equipped with a ×100 objective (Neofluar; numerical aperture = 1.3, Zeiss). For excitation, the 514-nm line of an Ar^+ laser (Innova 306, Coherent) running in TEM_{00} mode was coupled through an acoustooptic modulator (1205C-1; Isomet) into the epiport of the microscope. A $\lambda/4$-plate provided circular polarized excitation light. Using a defocusing lens (f = 100 mm) in front of the dichroic mirror (515DRLEXT02; Omega) the Gaussian excitation profile was set to 6.1 ± 0.8 μm full-width-at-half-maximum (FWHM) and 57 ± 15 kW/cm^2 mean excitation intensity. Illumination time for each image shown was 5 ms. After long-pass filtering (570DF70 Omega and OG550-3 Schott) the fluorescence was detected by a liquid-nitrogen-cooled CCD-camera (AT200, 4 counts/pixel read-out noise; Photometrix) equipped with a TH512B chip, (512 × 512 pixel, 27 μm^2 pixel size; Tektronix). The point-transfer function of the microscope was found to be adequately described by a two-dimensional Gaussian intensity distribution of width Γ_{PTF} = 0.42 μm FWHM, as determined from images of 30-nm fluorescent beads (Molecular Probes). Thus, the diffraction-limited area is $\pi/4\ \Gamma_{PTF}^2 = 0.14\ \mu m^2$. The width of the intensity profiles found for single molecules $\Gamma = 0.48 \pm 0.08$ μm FWHM was larger than Γ_{PTF} where the additional broadening could be accounted for by molecular diffusion. For data acquisition, the CCD was used as a storage device, such that 12 successive images of 40 × 40 pixels could be taken by using a frameshift procedure allowing for

The publication costs of this article were defrayed in part by page charge payment. This article must therefore be hereby marked "*advertisement*" in accordance with 18 U.S.C. §1734 solely to indicate this fact.

Abbreviations: TRITC DHPE, *N*-(6-tetramethylrhodaminethiocarbamoyl)-1,2-dihexadecanoyl-*sn*-glycero-3-phosphoethanolamine, triethylammonium salt; POPC, palmitoyloleoylphosphocholine; FWHM, full-width-at-half-maximum; MSD, mean-square displacement.

repetition rates of up to 140 images per s. The camera provided trigger pulses for the acoustooptic modulator for repeated illuminations, while the slow shutter of the camera was held open during the whole illumination sequence.

A test of the mechanical stability (17) of our apparatus was carried out by taking consecutive images of fluorescent latex spheres (30 nm; Molecular Probes) immobilized on a coverslip. Analysis of the positions of the spheres gave no indication for resolvable mechanical drifts on a time scale of seconds. The positions of the spheres were Gaussian distributed with a standard deviation of 12 nm, which compares well with 15 nm, the uncertainty of determination of their position by Gaussian fits.

RESULTS AND DISCUSSION

Fig. 1*A* shows fluorescence images of a (6.8 × 6.8) μm^2 membrane area for the highest, intermediate, and lowest dye density applied in this study. From these images, the mean signal in an area of 4 μm^2 at the image center was determined and divided by the number of dye molecules within this area. A mean value of (172 ± 15) counts per dye molecule was found for six dye densities covering the range from 10 to 10^3 dyes/μm^2. This value represents a quantitative prediction for the intensity of an image of an isolated labeled lipid. At 10 dyes/μm^2 a critical density is reached for which one dye molecule, on average, is found per diffraction-limited area of

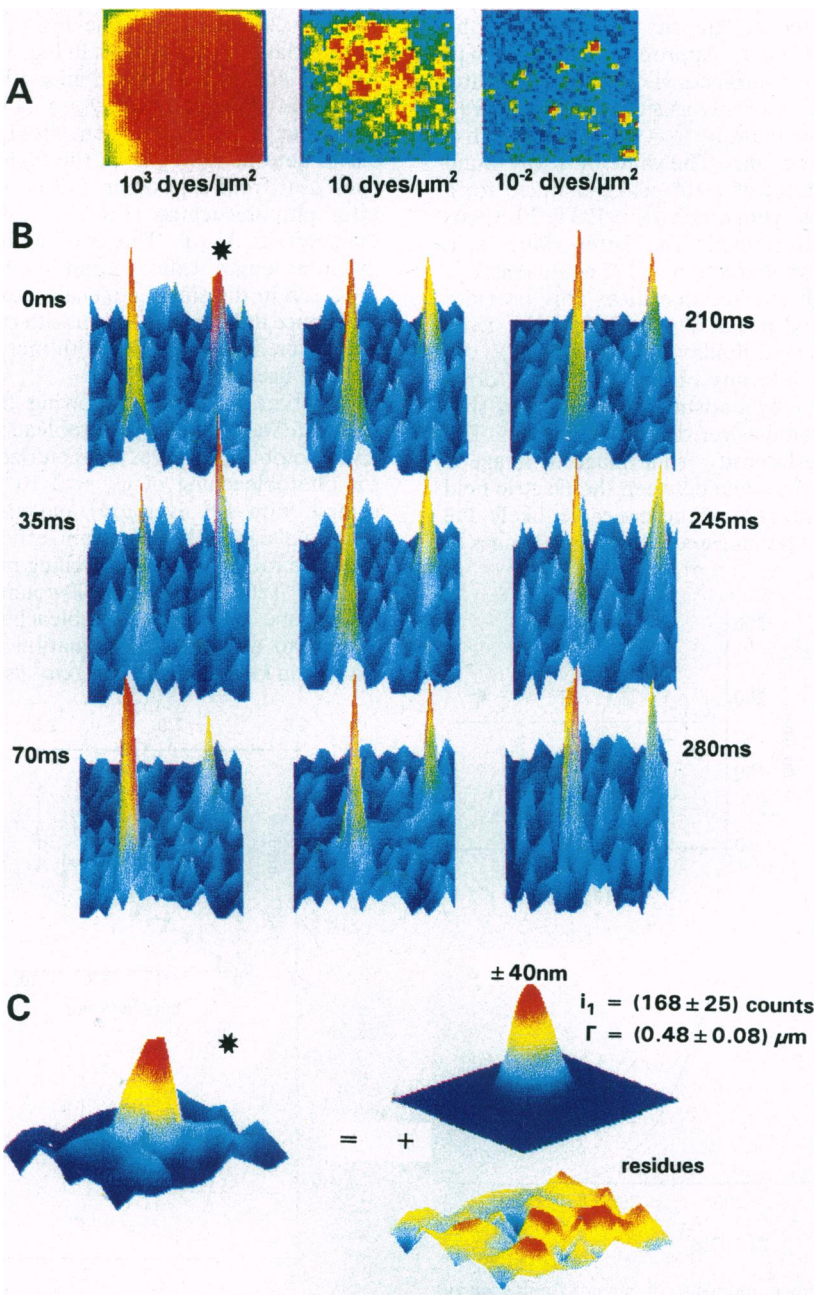

FIG. 1. Images of fluorescence-labeled lipids in a lipid membrane. The samples were illuminated for 5 ms with a Gaussian-shaped laser beam of 6.1 μm width and 57 kW/cm^2 mean excitation intensity. (*A*) Fluorescence images for three surface densities of labeled lipid. The images show a membrane area of 6.8 × 6.8 μm^2. Color scaling (blue = 0; red = 60 counts) is identical for the three images presented. Image intensity at 10^3 dyes/μm^2 was divided by 60. (*B*) Sequence of nine images of two labeled lipids observed at lowest surface density in a 5.4 × 5.4 μm^2 membrane area, taken every 35 ms. (*C*) Subimage of a 2.4 × 2.4 μm^2 membrane area showing the peak marked by * in *B*. The nonlinear least-squares fit of a two-dimensional Gaussian profile (18) to the peak yielded the indicated values for fluorescence intensity i_1, width and two-dimensional position with their respective confidence limits (see *Materials and Methods*). Residues of the fit compare with background noise.

the microscope. Images at this density were characterized by large fluctuations of the intensity as shown in Fig. 1*A*. For still lower dye densities, intensity fluctuations occurred as isolated peaks as shown for 10^{-2} dyes/μm^2 in Fig. 1*A*. Such isolated peaks were considerably more intense than the background. This is shown for two isolated peaks in the sequence of images presented in Fig. 1*B*. The sequence was obtained from consecutive illuminations of the same membrane area lasting 5 ms at 35-ms intervals. Three parameters of such peaks, their intensity i_1, width Γ, and position in the membrane plane were obtained from fitting Gaussian profiles to the peaks (18). Note that the Gaussian profile properly matches the point-transfer function of the optics used (see also *Materials and Methods*). Such analysis is exemplified in Fig. 1*C* (for the signal marked by * in Fig. 1*B*). Its fluorescence intensity, i_1, throughout the sequence is plotted in Fig. 2 (*Inset*). Appropriate summation of the intensities including their variances yields the probability-density distribution of peak intensity as shown in Fig. 2 (19). This distribution has a maximum at $\overline{i_1}$ = 154 counts with a standard deviation σ_1 = 53 counts. The value of $\overline{i_1}$ was found to be representative of a total of $>10^4$ peaks analyzed for a large number of membranes, from which $\langle\overline{i_1}\rangle = 173 \pm 20$ counts per dye molecule was determined. The latter value is in excellent agreement with the prediction of 172 counts per dye molecule obtained at high surface densities. This provides confidence that the isolated peaks observed originate from individual fluorescence-labeled lipids.

The uncertainty of each intensity value (Fig. 2 *Inset*, error bars) is fully accounted for by statistical errors due to shot noise, pixelation, and diffusion as verified by simulations. The additional variation of the intensity from image to image is attributed to variations of the angle between the electric field and the transition dipole moment of the molecule, likely due to surface corrugations as seen in force microscopy images of the glass surfaces used.

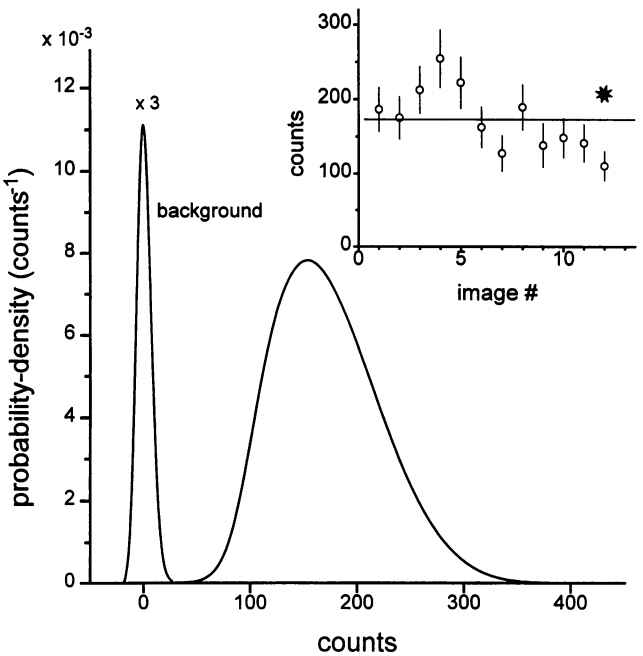

FIG. 2. Unitary fluorescence intensity of single fluorescence-labeled lipid molecules. The probability-density distribution of single molecule fluorescence intensity is shown. The probability-density distribution is calculated from data shown in the *Inset* as a superposition of normalized Gaussians, each entering at i_1 with a width given by the error bar. For comparison, the probability-density distribution of the background noise is shown. (*Inset*) Fluorescence intensity of the molecule marked by * in Fig. 1*B* as it progressed throughout the image sequence as determined by Gaussian fits (Fig. 1*C*).

The two lipid molecules observed in Fig. 1*B* undergo motion as it is apparent from the lateral shifts of the peaks in the image sequence. The position of a single molecule during each illumination was determined from Gaussian fits (Fig. 1*C*). The uncertainty was 30 nm, on average, which is 7 times smaller than the diffraction limited width of the optics used. This positional accuracy allowed us to visualize the trajectory of individual fluorophore movements for time intervals of 35 ms as shown in Fig. 3 for the two molecules in Fig. 1*B*. The observed displacements of the lipids conforms with two-dimensional Brownian diffusion in the membrane. Analysis of trajectories of 531 individual molecules showed that the direction of diffusional steps of simultaneously observed molecules were uncorrelated. The mean-square displacement (MSD) (20), and the time lag (t_{lag}) yielded the expected linear relationship as shown in Fig. 3 (*Inset*). Using the relation MSD = $4D_{lat}t_{lag}$ (21), the lipid motion is characterized by the lateral diffusion constant $D_{lat} = (1.42 \pm 0.13) \times 10^{-8}$ cm^2/s. This value is in fair agreement with $D_{lat} = (0.77 \pm 0.13) \times 10^{-8}$ cm^2/s determined by us at the highest surface density of 10^3 dyes/μm^2 from experiments using the fluorescence recovery after photobleaching (FRAP) technique (22) with a spot diameter of 3 μm. The two methods analyze diffusion at different length scales: $\approx$3 μm in our FRAP experiments and $\approx$0.3 μm in the single molecule experiments. The factor of 2 difference in D_{lat} is consistent with the general finding that D_{lat} values for lipids decrease with increasing length scale of the method used (23).

The time period of following the trajectory of a single molecule was limited by photobleaching of the fluorophor (24, 25). Photobleaching was characterized by a quantum efficiency for photobleaching of $\phi_b \approx 2\ 10^{-6}$, as determined from a sample with 10^3 dyes/μm^2 and also estimated from single molecule data. This quantum efficiency agrees with values reported for rhodamine bleaching ranging between $\phi_b = 10^{-5}$ and 10^{-7} (26, 27). About 4000 counts were collectable from a single labeled lipid before bleaching occurred. This corresponds to an overall illumination time of $\approx$120 ms at the excitation intensity of 57 kW/cm^2 used in this study. Bleaching

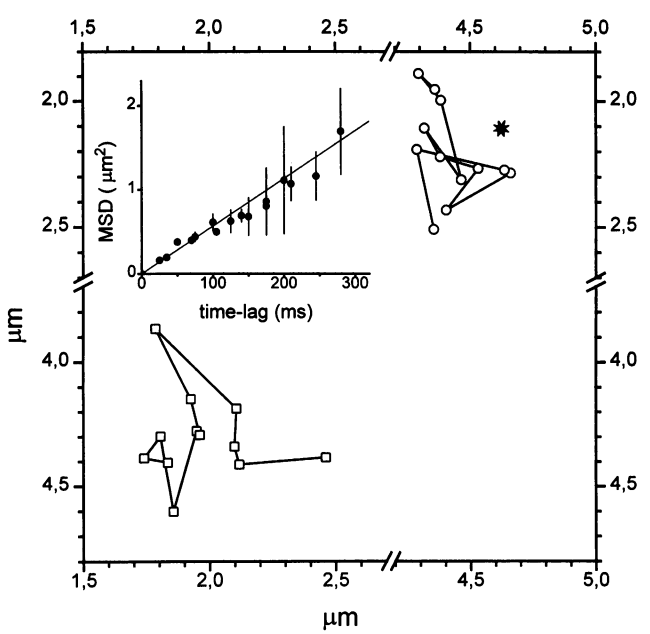

FIG. 3. Diffusion of single lipid molecules. Trajectories of the two-dimensional diffusion for the two lipid molecules in Fig. 1*B* determined from 12 successive images. (*Inset*) MSD versus time lag calculated for 531 trajectories. Observed displacements are consistent with two-dimensional Brownian diffusion of the lipids, since the data follow a linear relationship (solid line) well within their variance.

occurred in a one-step process for the present time resolution of 35 ms, which is taken as an additional fingerprint for single molecule observation (14, 28).

Single molecule imaging as described here can be characterized by two figures of merit. The first is the signal/noise ratio for detection of single dye molecules, which is defined as $(S/N) = \overline{(i_1)}/\sigma_b$, where σ_b is the standard deviation of the background intensity. Its distribution is included in Fig. 2 for comparison and is characterized by a standard deviation of $\sigma_b = 6$ counts, essentially due to CCD readout noise. This yields a signal/noise ratio of 28. The high reliability for detection using a 5-ms illumination time permitted for experiments at considerably shorter illumination times (not shown). For example, single dye molecules were still detectable with $(S/N) \approx 3$ at an illumination time of only 0.5 ms. The second figure of merit is given by $(\overline{i_1}/\sigma_1)^2$, representing the "stoichiometric resolution" of the method. It describes its potential for the study of stoichiometries—for example, in applications to biological systems by the use of fluorescence-labeled ligands like antibodies. Considering a number, n, of colocalized fluorescence-labeled ligands, the intensity, $\overline{i_n}$, and standard deviation, σ_n, of their fluorescence is expected to be $\overline{i_n} \pm \sigma_n = n\overline{i_1} \pm \sqrt{n}\sigma_1$. By *a priori* knowledge of the unitary intensity $\overline{i_1}$, the number n can be determined as long as the error $\sqrt{n}\sigma_1$ is smaller than $\overline{i_1}$ or for n smaller than $(\overline{i_1}/\sigma_1)^2$. Therefore, $(\overline{i_1}/\sigma_1)^2$ sets the limit in determining the number or stoichiometry of colocalized dye molecules. From the values found for the unitary intensity $\overline{i_1}$ and for σ_1, the method appears to have the potential for a stoichiometric resolution of up to $n = 8$ molecules.

CONCLUSIONS

Single lipid molecules carrying one fluorescence label were reliably detected by conventional fluorescence imaging at millisecond time resolution. Single dye images showed reproducibly a unitary fluorescence intensity of 173 counts at the illumination conditions applied. Due to the high image contrast, given by (S/N) = 28, small diffusional steps of individual lipids in the membrane plane could be resolved with 30-nm precision. Trajectories showed that lipid motion occurs random with MSDs described by a lateral diffusion constant of $D_{lat} = 1.42 \times 10^{-8}$ cm^2/s. The accuracy in detecting unitary fluorescence intensities led to the definition of a stoichiometric resolution which describes a novel potential for optical microscopy. Since the method widens the application range of single molecule microscopy from immobile to mobile systems, one field of application is bioscience—for example, the surface of living cells. In approaches used so far, biological ligands were employed, carrying many dye molecules (17, 18, 20, 22, 29, 30). This allowed to visualize dynamical processes occurring at living cell surfaces. However, there is a need for fluorescence microscopy, which enables us to resolve processes both in time and at the single molecule level with stoichiometric resolution. Such novel insights may be obtained by the method presented using monolabeled fluorescence ligands like antibodies or other compounds used by nature for molecular recognition.

This work was supported by the Austrian Research Fonds, Project S06607-MED.

1. Binnig, G., Rohrer, H., Gerber, Ch. & Weibel, E. (1982) *Physica* **110B,** 2075.
2. Binnig, G., Quate, C. F. & Gerber, Ch. (1986) *Phys. Rev. Lett.* **56,** 930–933.
3. Frommer, J. (1992) *Angew. Chem. Int. Ed. Engl.* **31,** 1298–1328, and references therein.
4. Bates, D. & Benderson, B., eds. (1993) *Advances in Atomic, Molecular and Optical Physics*, Vol. 31.
5. Shera, E. B., Seitzinger, N. K., Davis, L. M., Keller, R. A. & Soper, S. A. (1990) *Chem. Phys. Lett.* **217,** 553–557.
6. Rigler, R., Windengren, J. & Mets, Ü. (1992) in *Fluorescence Spectroscopy*, ed. Wolfbeis, O. (Springer, Berlin), pp. 13–24.
7. Whitten, W. B., Ramsey, J. M., Arnold, S. & Bronk, B. V. (1991) *Anal. Chem.* **63,** 1027–1030.
8. Nie, S., Chiu, D. T. & Zare, R. N. (1994) *Science* **266,** 1018–1021.
9. Kador, L., Horne, D. E. & Moerner, W. E. (1989) *Phys. Rev. Lett.* **62,** 2535–2538.
10. Orrit, M. & Bernard, J. (1990) *Phys. Rev. Lett.* **65,** 2716–2719.
11. Wild, U. P., Güttler, F., Pirotta, M. & Renn, A. (1994) *Chem. Phys. Lett.* **193,** 451–455.
12. Basché, Th. & Moerner, W. E. (1993) *Agnew. Chem. Int. Ed.* **32,** 457–476, and references therein.
13. Betzig, E. & Chichester, R. J. (1993) *Science* **262,** 1422–1425.
14. Funatsu, T., Harada, Y., Tokunaga, M., Saito, K. & Yanagida, T. (1995) *Nature (London)* **374,** 555–559.
15. Tamm, L. K. & McConnel, H. M. (1985) *Biophys. J.* **47,** 105–113.
16. Selig, J. (1981) in *Physical Properties of Model Membranes and Biological Membranes*, ed. Balian, R. (North Holland, Amsterdam), pp. 16–78.
17. Ghosh, R. N. & Webb, W. W. (1994) *Biophys. J.* **66,** 1301–1318, and references therein.
18. Gelles, J., Schnapp, B. J. & Sheetz, M. P. (1988) *Nature (London)* **331,** 450–453.
19. Bevington, P. R. & Robinson, D. K. (1992) *Data Reduction and Error Analysis for the Physical Sciences* (McGraw-Hill, New York).
20. Kusumi, A., Sako, Y. & Yamamoto, M. (1993) *Biophys. J.* **65,** 2021–2040.
21. Saffmann, P. G. & Dellbrück, M. (1975) *Proc. Natl. Acad. Sci. USA* **72,** 3111–3113.
22. Tsay, T. T. & Jacobson, K. A. (1991) *Biophys. J.* **60,** 360–368.
23. Vaz, W. L. C. & Almeida, P. F. (1991) *Biophys. J.* **60,** 1553–1554.
24. Hirschfeld, T. (1976) *Appl. Opt.* **15,** 3135–3139.
25. Peck, K., Stryer, L., Glazer, A. N. & Mathies, R. A. (1989) *Proc. Natl. Acad. Sci. USA* **86,** 4087–4091.
26. Rosenthal, I. (1978) *Opt. Commun.* **24,** 164–166.
27. Huston, A. L. & Reimann, C. T. (1991) *Chem. Phys.* **149,** 401–407.
28. Ambrose, W. P., Goodwin, P. M., Martin, J. C. & Keller, R. A. (1994) *Phys. Rev. Lett.* **72,** 160–163.
29. Käs, J., Strey, H. & Sackmann, E. (1993) *Nature (London)* **368,** 226–229.
30. Perkins, T. T., Quake, S. R., Smith, D. E. & Chu, S. (1994) *Science* **264,** 822–826.